Journal of Visualization, Vol. 8, No. 3 (2005)261-268

Combined Stereoscopic Particle Image Velocimetry and Line Integral Convolution Methods:

Application to a Sphere Sedimenting Near a Wall in a Non-Newtonian Fluid

Lawson, N. J.*[1], Finnis, M. V.*[1], Tatum, J. A.*[2] and Harrison, G. M.*[2]

*1 School of Engineering, Cranfield University, Cranfield, Bedfordshire MK43 0AL, U.K.
E-mail: n.lawson@cranfield.ac.uk
*2 Department of Chemical Engineering, Clemson University, Clemson SC 29634, U.S.A.

Received 21 October 2004
Revised 17 January 2005

Abstract : The flow fields for a sphere sedimenting through a Newtonian and two non-Newtonian liquids near a wall in a square tank are investigated using 3-D stereoscopic particle image velocimetry (PIV) and line integral convolution (LIC) methods. The PIV data were taken using an angular stereoscopic configuration with tilt and shift arrangements for the Scheimpflug condition and a pair of liquid correction prisms. Data were recorded from planes perpendicular and parallel to the wall for each fluid case over a range of distances from the wall. The PIV and LIC results highlight significant differences in the wake structure for all three cases. Out of plane flow was also found to persist up to two sphere diameters downstream in the wake for all cases.

Keywords : Visualization, Stereoscopic PIV, LIC, Non-Newtonian.

1. Introduction

Modeling non-Newtonian fluid flows is regarded as a significant challenge both theoretically and numerically. Selected experimental cases, such as the sedimentation of a sphere through a quiescent polymer solution, have aimed to provide validation data for the numerical methods (Hassager, 1988). In the majority of previous work, centerline sedimentation of a sphere is recorded in an axisymmetric tank (e.g., see Tanner, 1963, Chhabra et al., 1980, Chmielowski et al., 1990). Alternatively, a more challenging case, which is now gaining attention, is the sedimentation of a sphere near a vertical wall (e.g. see Joseph et al., 1994, Becker et al., 1996).

Flow visualisation has been used to investigate non-Newtonian sedimentation flow fields (Sigli and Coutanceau, 1977). Advanced techniques such as laser Doppler anemometry (LDA) and particle image velocimetry (PIV) (Adrian, 1991, Kim et al., 2002, Yu-Cheong et al, 2002) have also been used to measure the flow field surrounding the sedimenting sphere (Bush 1993, 1994, Arigo and McKinley, 1998).

Recently, flow visualization data has been obtained for the more complex example of a sphere sedimenting near a wall (Joseph et al., 1994, Becker et al., 1996, Singh and Joseph, 2000). These experiments have demonstrated unusual flow effects such as sphere rotation and migration towards and away from the wall. Harrison et al. (2001) have studied a sphere sedimenting near a planar wall

with 3-D stereoscopic PIV. In this case, sphere rotation and migration were not observed, but significant fluid motion perpendicular to the wall was recorded.

More recently, to aid visualization of complex flow fields, PIV has been combined with line integral convolution (LIC) methods (Cabral and Leedom, 1993) as demonstrated by Longmire et al. (2003). In the following, angular stereoscopic PIV and LIC methods are used to study the sedimentation flow field from a Newtonian reference fluid, a constant shear viscosity (elastic) Boger fluid and a shear thinning fluid. To the authors knowledge, this is the first time PIV and LIC methods have been combined to aid the flow visualization of a non-Newtonian flow.

2. Experimental Methods

2.1 PIV Test Rig

Figure 1 shows the stereoscopic PIV set-up. The system is based on an angular viewing arrangement with tilt and shift mounts to obtain the Scheimpflug condition. Pairs of liquid correction prisms are mounted on the tank for minimum image distortion (Prasad and Jensen, 1995). The camera semi-angle was set to between $\alpha = 15^o - 25^o$ for optimum performance with an expected error ratio of around 3.5 (Lawson and Wu, 1997). The liquid prisms were set at 15^o to correspond with the minimum camera angle and filled with an approximately 50/50 water glycerol solution for refractive index matching. By employing two pairs of prisms mounted on the tank (as shown in Figs. 1a) and 1b)) flow field measurements in planes both parallel to and perpendicular to the wall were obtained. The test tank had dimensions 200 mm (l) × 200 mm (w) × 500 mm (h).

Two independent PIV systems were used to acquire the data. The first system was based on a pair of Kodak ES1.0 CCD's (8 bit 1008 x 1018 pixels) with a New Wave Gemini Nd:YAG pulsed laser system (120 mJ/pulse) and was employed for the shear-thinning fluid. For both the Newtonian and Boger fluids a pair of NAC HiDCAM II high speed digital CMOS cameras (8 bit 1240 x 1024 pixels at 500 frames per second) with a Photonics Industries GM30-5270E Nd:YLF pulsed laser (25 mJ/pulse) was employed. The acquisition process for both systems was triggered by monitoring a trigger laser beam placed in the path of the sedimenting sphere with a variable time delay before triggering.

To improve the image quality on both sides of the sphere, a 0.5 mm thick dual light sheet system was generated as shown in Fig. 1. Also, to reduce reflections off the sphere surface, the flow was seeded with fluorescent Rhodamine 6G particles and the images viewed through a Kodak Wratten number 21 gel filter. The particle size range was between 75 μm–120 μm and seeding density corresponded to around 6-10 particles images per interrogation volume.

2.2 Test Fluids

Three different test fluids were employed: a Newtonian reference fluid, a constant shear viscosity (elastic) Boger fluid and a shear thinning fluid. All fluids have similar zero shear viscosities. The Weissenberg and Reynolds numbers were manipulated by varying both the diameter (2.38 mm, 6.35 mm, and 9.53 mm) and the sphere specific gravities over the range 2.45 and 8.03 with glass and steel respectively. In all fluids, each sphere was dropped at one diameter from the wall to the edge of the sphere at terminal velocity. For each of the experiments a characteristic shear rate was determined by dividing the terminal velocity by the sphere diameter. The Weissenberg and Reynolds numbers were determined using the terminal velocity.

The Newtonian baseline fluid, over the broad range of shear rates, had a viscosity of 175 Pa*s. The Boger fluid had a constant shear viscosity of about $\eta = 30$ Pa*s. The shear rheology for the shear-thinning fluid showed a zero shear viscosity of 14 Pa*s with the first normal stress coefficient being marginally greater than the Boger fluid. More details of the fluid rheology may be found in Tatum et al. (2004).

Table 1 summarizes the conditions employed for the experiments reported in this work.

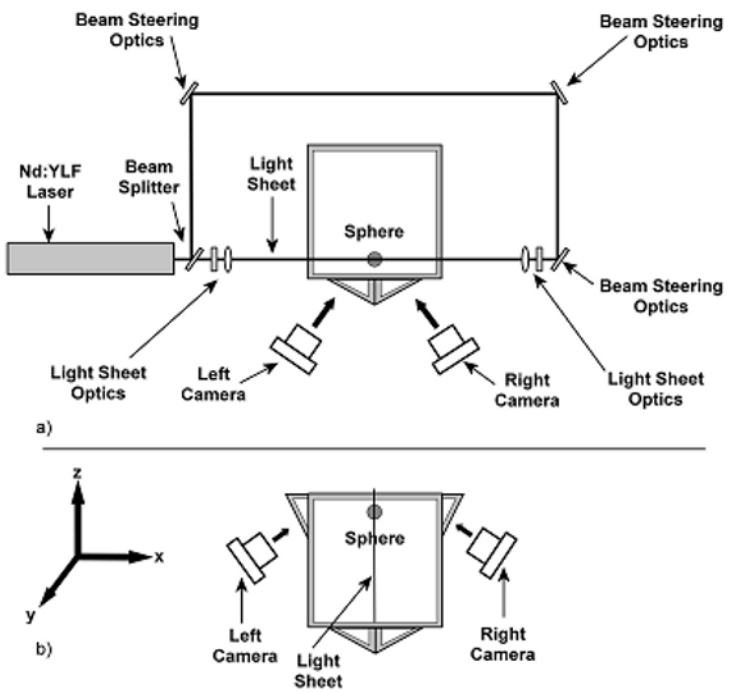

a) Parallel wall measurements b) Perpendicular wall measurements
Fig. 1. PIV experimental setup.

Table 1. Summary of Experimental Conditions (NF – Newtonian Fluid, BF – Boger Fluid, STF – shear thinning fluid, SV – Side View).

Name	Diameter (mm)	Material	Wall Distance	Velocity (mm/s)	Shear Rate (s^{-1})	Reynolds Number	Weissenberg Number
NF.2	6.35	Metal	1	0.697	1.10E-01	3.73E-05	N/A
BF.1	6.35	Glass	1	1.14	1.80E-01	3.43E-04	2.79E-02
BF.4	6.35	Glass	1 (SV)	1.14	1.80E-01	3.43E-03	2.79E-02
STF.3	9.53	Metal	1	83.5	1.32E+01	6.58E-02	2.41E+00

2.3 PIV Data Processing

Stereoscopic data processing was completed using ILA VidPIV software. The calibration procedure used images of a test grid with 2.5 mm diameter black dots on a 2.5 mm square with 9 separate grid translations at out of plane positions 0, ±8, ±15, ±50 and ±100% of the sphere diameter. PIV data processing was completed with a 16 x 16 pixel cross-correlation followed by an adaptive cross correlation all with a 50% overlap. Data were globally filtered, interpolated and smoothed with a Gaussian kernel before calculating the 3C data. Further post processing of the PIV data involved overlapping average vector maps with 20 samples each at different time delays. Estimated in plane and out of plane errors are 2.1% and 7.8% respectively both at full scale (see Prasad, 2000).

2.4 LIC Methods

Line integral convolution (LIC) is an image processing technique that allows visualization of a vector field. Cabral and Leedom (1993) first presented the technique in this context and since then it has been used as a general tool for visualizing vector fields. The technique involves locally filtering an image along field lines giving directional information at a high spatial resolution. Using white noise as the starting image, LIC can produce images reminiscent of particle suspension visualization of

water flows. The implementation of LIC used in the following relies on a vector field defined on a regular grid obtained as described in section 2.3. The implementation is resolution independent in that the number of pixels of the image is independent of the grid on which the vectors are defined, in a similar manner to the implementation of Stalling and Hege (1995). (Although in our implementation the number of pixels per grid cell was restricted to an integer value.) Within each grid cell bilinear interpolation was used to evaluate vector values. The integration was performed using a 4th order Runge-Kutta formula with an embedded 3rd order formula allowing an adaptive step size to be used to maintain a given solution tolerance. In addition the method provided an interpolation which enabled accurate transition between grid cells. Essentially the method consists of integrating forwards and backwards a given distance along the streamline starting at the centre of each pixel. The pixel values of each pixel in the input image that lies under the integrated streamline are averaged and the resulting value forms the corresponding pixel in the output image. In order to enhance the LIC image we use a multi-pass method similar to that described by Okada and Kao (1997). For a given vector field we apply LIC firstly to a white noise image, secondly to the output image of the first pass and finally to the sharpen-filtered histogram-equalised output image of the second pass. This results in an image that is qualitatively better than that of the single pass LIC.

In the following we also combine the LIC data with a coloured contour image to indicate velocity magnitude where red represents maximum velocity and black minimum velocity.

3. Results and Discussion

3.1 Newtonian Fluid

Figure 2 shows a PIV vector map (in the image plane defined by Fig. 1a)) and a corresponding LIC image for the 6.35 mm metal sphere sedimenting in the Newtonian fluid one ball diameter from the wall. The sphere has a settling velocity of 0.697 mm/s. This Newtonian flow was used as a benchmark flow for comparison with the other two non-Newtonian flows. Recirculation zones either side of the sphere can be clearly seen centred around x/D = ±3D and y/D = 0, along with a wake extending downstream of the sphere. The wake appears to extend to at least 4D downstream of the sphere and ±2D either side of the sphere. Visually the LIC image provides greater clarity than the PIV plots when isolating this type of flow structure. The addition of the background contours for velocity magnitude also greatly enhances the global information which the viewer has available.

Examining the quantitative data in more detail, although the recirculation structure extends beyond the field of view, it falls to less than 2% of the sphere terminal velocity V_t at y/D = 0.5D and x/D = ±3.0D. The peak vertical component of fluid velocity recorded in this case was around 12% of V_t at y/D = 1.0D and x/D = ±1.0D. At 4.5D the presence of the recirculation zone is undetectable within experimental error. If the wake decay is also analyzed in more detail, consideration of the vertical component of velocity shows the wake to falling rapidly from nearly 70% of V_t at y/D = 0.5 to around 12% of V_t at y/D = 3.0.

Analysis of the 3C stereoscopic data showed that the effect of the wall was to generate substantial motion perpendicular to and away from the wall. In this case, peak out of plane velocities were found to be around 20% of the terminal velocity, V_t.

3.2 Boger Fluid

Figure 3 shows two LIC images for the Boger fluid. View a) reports a measurement plane parallel to the wall and view b) shows a view perpendicular to the wall. In both experiments the laser passes through the ball centreline. The Boger fluid is used to investigate the effect of elasticity by addition of a low concentration of polymer in the fluid. Careful selection of corn syrup as the base fluid also ensured negligible shear thinning effects.

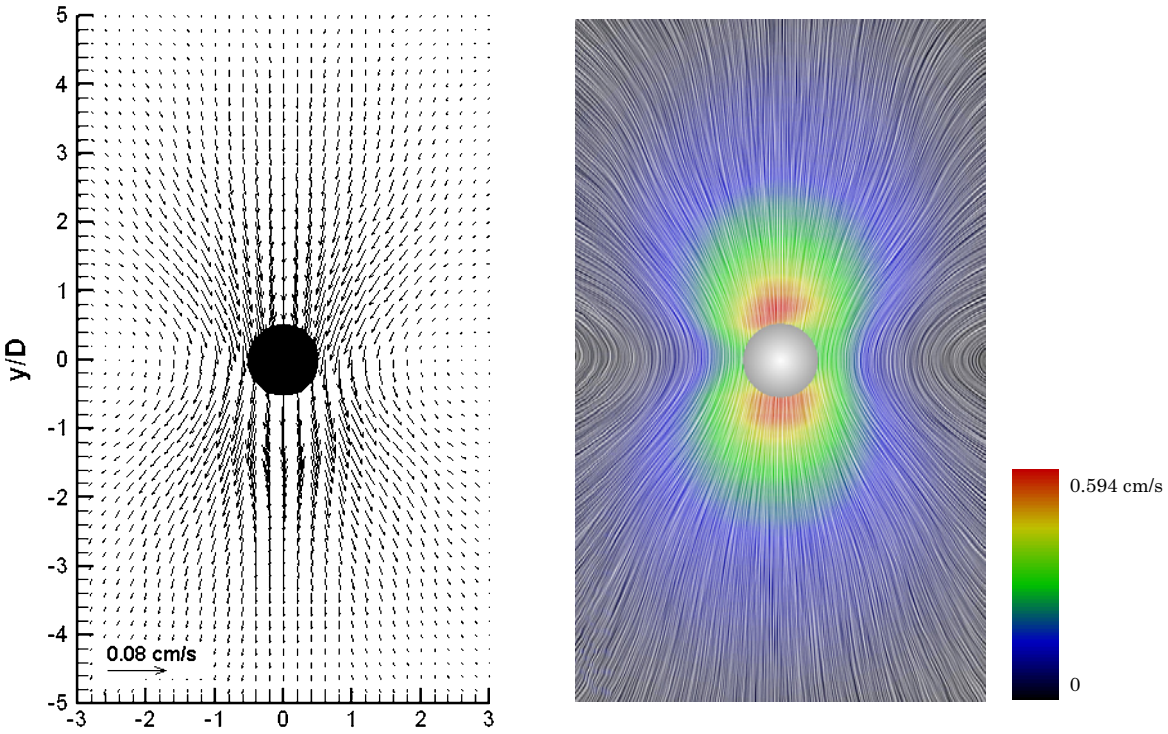

a) PIV Vector Map b) LIC Image

Fig. 2. Data from Newtonian Fluid (6.35 mm metal ball, 1 diameter from wall).

If the view parallel to the wall is considered first, as with the Newtonian fluid recirculation zones, structures either side of the sphere are clearly evident and are centered at approximately y/D = 0. Comparison of the Boger fluid PIV data with the corresponding Newtonian fluid data shows the peak velocities in the zones to be approximately 40% lower than for the Newtonian flow with a peak velocity of the u component of around 7% of V_t. This significant reduction is attributed to the effect of elasticity as Reynolds number in both cases is low and in the creeping flow regime, i.e., Re < 0.01 resulting in a dominant effect of viscous forces over inertial forces.

Considering the view in which the laser sheet is perpendicular to the wall (Fig. 3b)), the influence of the wall on the left hand side of the image is clearly visible as only a single recirculation zone is now present at z/D = 5.0. This flow structure also generates the substantial motion perpendicular to the wall as found in the PIV data which ranges from between 5% of V_t for the Boger fluid to 20% of V_t for the Newtonian fluid. The lower motion perpendicular to the wall in the case of the Boger fluid is thought to be caused by the narrowing of the wake due to the effects of elasticity. This narrowing is evident from direct comparisons with the Boger fluid at the $1/e^2$ value of v/V_t which show the wake to have 30% less width than the Newtonian fluid.

3.3 Shear-Thinning Fluid

Figure 4 shows a LIC image of the shear thinning fluid taken in a plane parallel to the wall about the centerline of the sphere. The shear thinning fluid has a viscosity dependent on shear rate along with a degree of elasticity. Therefore isolation of the different fluid characteristics is more complex.

The wake and recirculation zones are clearly visible where the latter flow structure is positioned at around x/D = ±2.5D and y/D = 0. Thus the shear thinning effect is to partially offset the effect of elasticity as the equivalent point in the flow field of the Boger fluid is nearer to the sphere (Fig. 3). The result of the recirculation zones moving away from the sphere is also to lengthen and widen the wake. However, the width of the wake of the shear-thinning fluid extends less in the

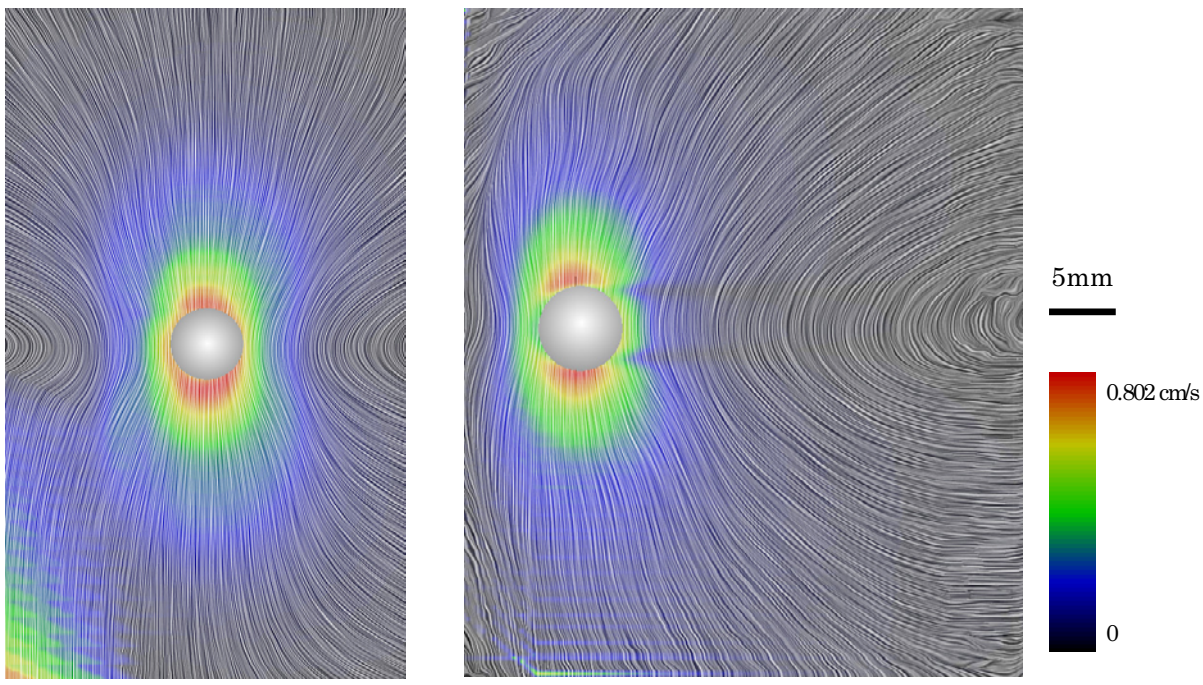

a) Measurement plane parallel to wall b) Measurement plane perpendicular to wall

Fig. 3. LIC images from a Boger Fluid (6.35 mm (a), 6.35 mm (b) diameter glass ball, 1 diameter from wall).

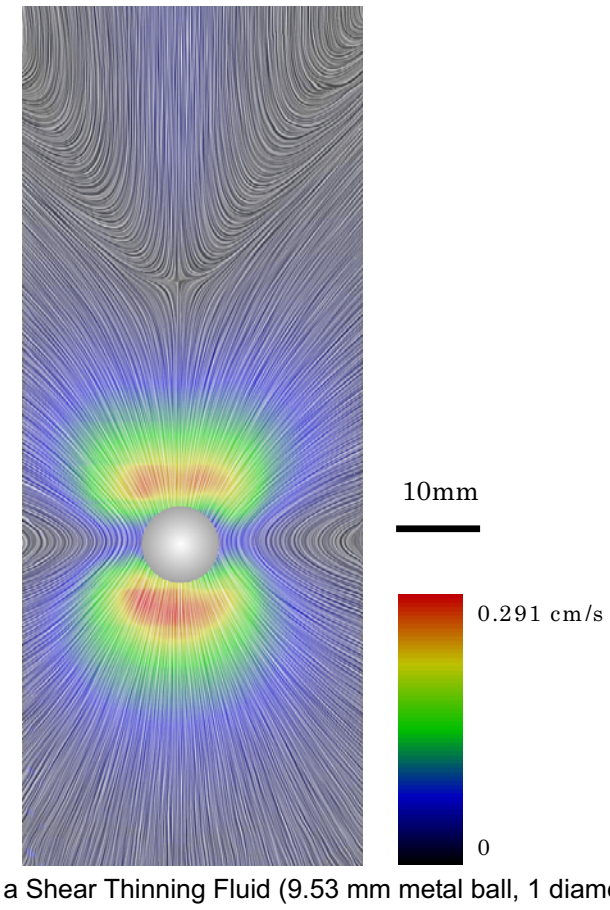

Fig. 4. LIC image from a Shear Thinning Fluid (9.53 mm metal ball, 1 diameter from wall).

lateral direction than observed for the Newtonian fluid and is due to the competing effects of elasticity and shear thinning within the shear-thinning fluid.

A "negative wake" flow structure is generated behind the sphere: downstream of the sedimenting sphere the fluid actually flows in the positive y direction (i.e., in the opposite direction from the sphere). In this case the negative wake starts to appear at 3.5-3.8 ball diameters behind the center of the sphere depending on the Weissenberg number. In this region, the magnitude of the negative wake is much smaller than that of the flow in the immediate vicinity of the sphere and the negative wake is dominated by the vertical component of velocity. The LIC image technique provides the clearest visualization of the position and structure formation of the negative wake.

4. Conclusion

This work has presented detailed flow visualization of the fluid motion generated by a sphere sedimenting one diameter from a wall in a number of non-Newtonian fluids and a reference Newtonian fluid. This flow presents a challenging test case in non-Newtonian fluid mechanics for numerical modelers. The image processing technique LIC was also used to enhance the recorded PIV data. Results showed the effect of elasticity in the Boger fluid was to significantly reduce the width of the wake by 30% and greatly reduce the peak recirculation velocity by 40% with a corresponding decrease in out of plane velocities from 20% in the Newtonian test case to less than 5% in the Boger fluid. Through studies with the shear-thinning fluid it is shown that only through a combination of shear-thinning and elastic effects is a negative wake produced.

Acknowledgements

This material is based upon work supported by the National Science Foundation under Grant No. INT-0309459.

References

Adrian, R. J., Particle-imaging techniques for experimental fluid-mechanics, Ann. Rev. Fluid Mech., 23 (1991), 261-304.

Arigo, M. T. and McKinley, G. H., An experimental investigation of negative wakes behind spheres settling in a shear-thinning viscoelastic fluid, Rheologica Acta, 37 (1998), 307-327.

Becker, L. E., McKinley, G. H. and Stone, H. A., Sedimentation of a sphere near a plane wall: weak non-Newtonian and inertial effects, J. of Non-Newtonian Fluid Mech., 63 (1996), 201-233.

Bush, M. B., The stagnation flow behind a sphere, J. of Non-Newtonian Fluid Mech., 49 (1993), 103-122.

Bush, M. B., On the stagnation flow behind a sphere in a shear-thinning viscoelastic liquid, J. of Non-Newtonian Fluid Mech., 55 (1994), 229-247.

Cabral, B. and Leedom, L. C., Imaging Vector Fields Using Line Integral Convolution, Computer Graphics (SIGGRAPH '93 Proceedings), J. T. Kajiya, Ed., 27 (1993-8), 263-272.

Chhabra, R. P., Uhlherr, P. H. T. and Boger, D. V., The influence of fluid elasticity on the drag coefficient for creeping flow around a sphere, J. of Non-Newtonian Fluid Mech, 6 (1980), 187-199.

Chmielowski, C., Nichols, K. L. and Jayaraman, K., A comparison of the drag coefficients of spheres translating in corn-syrup-based and polybutene-based Boger fluids, J. of Non-Newtonian Fluid Mech., 35 (1990), 37-49.

Harrison, G. M., Lawson, N. J. and Boger, D. V., The measurement of the flow around a sphere settling in a rectangular box using 3-dimensional particle image velocimetry, Chem. Eng. Comm., 188 (2001), 143-178.

Hassager, O., Working group on numerical techniques, J. of Non-Newtonian Fluid Mech., 29 (1988), 2-5.

Joseph, D. D., Liu, Y. J., Poletto, M. and Feng, J., Aggregation and dispersion of spheres falling in viscoelastic liquids, J. of Non-Newtonian Fluid Mech., 54 (1994), 45-86.

Kim, K. C., Lee, M. B., Yoon S. Y., Boo J. S. and Chun, H. H., Phase Averaged Velocity Field in the Near Wake of a Square Cylinder Obtained by a PIV Method, Journal of Visualisation, 5-1 (2002), 29-36.

Lawson, N. J. and Wu, J., Three-dimensional particle image velocimetry: experimental error analysis of a digital angular stereoscopic system, Meas Sci. Tech., 8 (1997), 1455-1464.

Longmire, E. K., Ganapathisubramani, B., Marusic, I., Urness, T. and Interrante, V., Effective visualization of stereo particle image velocimetry vector fields of a turbulent boundary layer, J. of Turb., 4 (2003), 023.

Mena, B., Manero, O. and Leal, L. G., The influence of rheological properties on the slow flow past spheres, J. of Non-Newtonian Fluid Mech., 26 (1987), 247-275.

Okada, A. and Kao, D. L., Enhanced Line Integral Convolution with Flow Feature Detection, Proceedings of IS & T/SPIE Electronics Imaging 97 (San Jose, California), v3017 (1997-2), 206- 217.

Prasad, A. K., Stereoscopic Particle Image Velocimetry, Exp. in Fluids, 29-2 (2000), 103-116.

Prasad A. K. and Jensen, K., Scheimpflug stereocamera for particle image velocimetry in liquid flows, Applied Optics, 34-30 (1995), 7092-7099.

Sigli, D. and Coutanceau, M., Effect of finite boundaries on the slow laminar isothermal flow of a viscoelastic fluid around a

spherical obstacle, J. of Non-Newtonian Fluid Mech., 2 (1977), 1-21.
Singh, P. and Joseph, D. D., Sedimentation of a sphere near a vertical wall in an Oldroyd-B fluid, J. of Non-Newtonian Fluid Mech., 94 (2000), 179-203.
Stalling, D. and Hege, H..-C., Fast and Resolution Independent Line Integral Convolution, Computer Graphics (SIGGRAPH '95 Proceedings), R. Cook, Ed., (1995), 249-256.
Tanner, R. I., End effects in falling-ball viscometer, J. of Fluid Mech., 17 (1963), 161-170.
Tatum J. A., Finnis M. V., Lawson, N. J. and Harrison, G. M., 3-D Particle Image Velocimetry of the Flow Field Around a Sphere Sedimenting Near a Wall. Part 1. Effects of Weissenberg Number, submitted to J. of Non-Newtonian Fluid Mech, (2004-3).
Yu-Cheong, I., Kobayashi, T., Saga, T. and Itoh, T., Stereoscopic PIV Measurements of Flow in and around Axial Flow Fan, Journal of Visualisation, 5-1 (2002), 51-58.

Author Profile

Nicholas J. Lawson: He received his Ph.D. in Mechanical engineering in 1995 from Loughborough University. After completing a post-doctoral assignment at the University of Melbourne, he joined the Department of Aerospace, Power and Sensors at Cranfield University in 1999 as a Lecturer before moving to the Department of Aerospace Sciences as a Senior lecturer in 2003. His research interests are the application and development of particle image velocimetry (PIV) and laser Doppler anemometry LDA techniques.

Mark V. Finnis: He received his Ph.D. in 1993 from Cranfield Institute of Technology. He works in the Department of Aerospace, Power and Sensors at the Royal Military College of Science, Cranfield University. His research interests are boundary-layer stability, wind-tunnel technology and external ballistics. He also has experience of wind tunnel flow measurement using PIV and LDA techniques.

Jared A. Tatum: He is a Ph.D. Candidate in the department of Chemical Engineering at Clemson University in Clemson South Carolina. Mr. Tatum received a BS with a double major in Chemical Engineering and Chemistry from Rose-Hulman Institute of Technology before beginning his Ph.D. candidacy. His research interests include: rheology of complex fluids, extensional properties of complex fluids, and optical techniques for complex fluid.

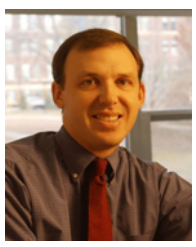

Graham M. Harrison: He received his Ph.D. in Chemical Engineering in 1997 from the University of California, Santa Barbara. After completing a post-doctoral assignment at the University of Melbourne, he joined the Dept. of Chemical Engineering at Clemson University in 1999 as an assistant professor. His research interests are Extensional Flow Properties and Optical Techniques for Non-Newtonian fluid mechanics.